Biosensors and Bioelectronics 126 (2019) 365–372

Contents lists available at ScienceDirect

Biosensors and Bioelectronics

journal homepage: www.elsevier.com/locate/bios

Biomolecular charges influence the response of surface plasmon resonance biosensors through electronic and ionic mechanisms

Hana Šípová-Jungová*[,1], Ludmila Jurgová, Kateřina Mrkvová, Nicholas Scott Lynn, Barbora Špačková[1], Jiří Homola*

Institute of Photonics and Electronics, Czech Academy of Sciences, Chaberská 57, 182 51 Prague, Czech Republic

ARTICLE INFO

Keywords:
Surface plasmon resonance
Surface charge
Biomolecules
Self-assembled monolayers of alkanethiols

ABSTRACT

Surface plasmon resonance (SPR) biosensors have become an important label-free optical biomolecular sensing technology and a "gold standard" for retrieving information on the kinetics of biomolecular interactions. Even though biomolecules typically contain an abundance of easily ionizable chemical groups, there is a gap in understanding of whether (and how) the electrostatic charge of a biomolecular system influences the SPR biosensor response. In this work we show that negative static charge present in a biomolecular layer on the surface of an SPR sensor results in significant SPR spectral shifts, and we identify two major mechanisms responsible for such shifts: 1) the formation of an electrical double layer (*ionic* mechanism), and 2) changes in the electron density at the surface of a metal (*electronic* mechanism). We show that under low ionic strength conditions, the electronic mechanism is dominant and the SPR wavelength shift is linearly proportional to the surface concentration of biomolecular charges. At high ionic strength conditions, both electric and ionic mechanisms contribute to the SPR wavelength shift. Using the electronic mechanism, we estimated the pKa of surface-bound carboxylic groups and the relative concentration of the carboxyl-terminated alkanethiols in a binary self-assembled monolayer of alkanethiols. The reported sensitivity of SPR to surface charge is especially important in the context of biomolecular sensing. Moreover, it provides an avenue for the application of SPR sensors for fast, label-free determination of the net charge of a biomolecular coating, which is of interest in material science, surface chemistry, electrochemistry, and other fields.

1. Introduction

Surface plasmon resonance (SPR) biosensing, established in the 1980s (Nylander et al., 1982), represents the most advanced label-free optical affinity biosensor technology. SPR biosensors utilize surface plasmon polaritons (SPP), i.e. charge density oscillations that propagate along the interface between a dielectric and metal (typically gold or silver), to probe processes occurring in the dielectric medium. SPPs exhibit a variety of useful properties, including electromagnetic field enhancements, localization to subwavelength dimensions, and high surface and bulk sensitivities (Barnes et al., 2003). Because of these attributes, SPPs have found applications in fields such as spectroscopy (Abb et al., 2014), nanophotonics (Berini and De Leon, 2012; Fang and Sun, 2015), and imaging (Kawata et al., 2009; Puiu and Bala, 2016). The establishment of compatible surface chemistries has enabled functionalization of the SPR surface with various biomolecular receptors, unlocking the potential of the SPR method for bioanalytical applications (Mariani and Minunni, 2014) and making SPR sensors a powerful tool for investigation into the kinetics of biomolecular interactions (Karlsson, 2004).

In the classical treatment of SPR biosensors, shifts in the SPR wavelength (or frequency) are proportional to changes in the molecular mass of bound molecules (de Feijter et al., 1978). A fundamental question (concerning any type of SPR biosensor) is whether, and how, the optical response is influenced by the buildup of charges (via captured biomolecules) on the SPR surface. This question is of paramount importance, as easily ionizable groups, such as primary amines or carboxyl moieties, are abundant in biomolecules and biomolecular coatings (Wijaya et al., 2011). The amine-coupling reaction (broadly used for the immobilization of protein ligands) serves as a good example: it involves replacement of a surface-bound carboxylic group with covalent bond, changing a potentially negative terminal group to a

* Corresponding authors.
E-mail addresses: hana.sipova@chalmers.se (H. Šípová-Jungová), homola@ufe.cz (J. Homola).
URL: http://www.ufe.cz (J. Homola).
[1] Present address: Department of Physics, Chalmers University of Technology, 412 96 Göteborg, Sweden.

https://doi.org/10.1016/j.bios.2018.11.002
Received 25 June 2018; Received in revised form 19 September 2018; Accepted 1 November 2018
Available online 06 November 2018
0956-5663/

neutral complex (Fischer, 2010).

There are two major mechanisms that can induce a plasmonic shift for a metal surface in contact with a simple electrolyte: an *ionic* mechanism, and an *electronic* mechanism. The *ionic* mechanism is associated with the formation of an electrical double layer above a (charged) biomolecular layer on the SPR surface, whereby the imbalance of ionic charges close to the surface acts to locally alter the refractive index, thus inducing a SPR shift. Fears et al. exploited this mechanism to measure the pKa of carboxyl- and amino- terminated alkanethiol self-assembled monolayers (SAM), where SPR shifts after surface charging (via titration in both CsCl and NaBr solutions) were solely attributed to the formation of a double layer capacitor (Fears et al., 2008).

The *electronic* mechanism is associated with changes in the density of conductive electrons within the metal layer in the proximity of the dielectric interface. Discussion of this mechanism has been reported in several works regarding the combination of SPR with electrochemical sensing (EC-SPR), specifically on the relationship between the electrochemical current (or potential) and the SPR response (Mcintyre, 1973; Wang et al., 2010). Further discussion can be found in the nanoplasmonic sensing literature, where Novo et al. linked shifts in localized surface plasmon resonance (LSPR) to changes in the electron density on surface-bound gold nanoparticles (via the electrochemical charging of such nanoparticles) (Novo et al., 2009). Nevertheless, there is still controversy in the interpretation of the LSPR shift due to the potential induced on the nanoparticles. While some researchers attribute it to the charging of the metal (Foley et al., 2008; Novo et al., 2009), others argue that this effect is small and link the observed plasmonic shift to the formation of chloride salts on the metal surface (Dahlin et al., 2012).

Discussion on either mechanism, however, is relatively miniscule when compared to the much larger body of work on SPR biosensors. Temporal changes in molecular surface charge are to some extent present in the vast majority of all SPR experiments documented in the current literature. Understanding of how these charges affect the SPR response is therefore crucial for the correct interpretation of SPR results, both for those related to interaction analysis as well as for purposes of biodetection.

In this study we investigate SPR shifts induced by the charge of immobilized biomolecules and furthermore, present experiments that allow us to distinguish between shifts induced by electronic and ionic mechanisms. To accomplish this, we modified the SPR surface with both carboxyl- and hydroxy- terminated self-assembled monolayers of alkanethiols (SAM_{COOH} and SAM_{OH}, respectively) that block any direct charge transfer between the solution and the metal. While SAM_{OH} form a compact molecular layer that is neutral over a large pH range (pH 2–10), the charge of SAM_{COOH} can be varied from neutral ($pH \ll pK_a$) to highly negative ($pH > pK_a$) by changing the pH of the bulk media. We track SPR wavelengths in various bulk solutions and compare the SPR shifts measured on both neutral and negatively charged SAMs. We found that deprotonation of the carboxylic moieties on SAM_{COOH} causes significant SPR shifts, even in buffers having very low ionic concentrations. We hypothesize that this shift is caused by an electronic mechanism, where the agreement of experimental results with a theoretical multilayer model (predicting SPR shifts when subjected to surface charges) serves to confirm such hypothesis. Furthermore, we study the ionic mechanism by monitoring SPR shifts in solutions of NaCl and $MgCl_2$, and we show that formation of a double layer causes an additional SPR shift.

2. Materials and methods

2.1. SPR sensor

We used a SPR sensor developed at the Institute of Photonics and Electronics (Prague, Czech Republic) based on the attenuated total reflection method and wavelength spectroscopy of surface plasmons (Šípová et al., 2012). In short, parallel beams of white light were used to excite surface plasmons on a thin gold or silver film in four areas, which were interfaced with four separate chambers of a flow cell (Su et al., 2005). We analyzed the light reflected from the gold layer with a spectrometer, where we tracked the spectral position of the intensity minimum corresponding to SPR wavelength. The SPR wavelength was set to 750 nm at the beginning of each experiment by adjusting the angle of incident light. Sample delivery was carried out via a microfluidic system that allows for near-dispersionless delivery of sample to the SPR chip (Špringer et al., 2010). The SPR sensor was equipped with Peltier temperature stabilization capable of maintaining the temperature within the flow cell with a precision of 0.01 °C. The temperature was set to 25 °C, and the flow-rate was kept at 20 μL/min. The SPR chip was made of a BK7 glass slide coated with an adhesion-promoting layer of titanium (thickness 1.5 nm) and a layer of gold (thickness 50 nm), deposited by electron beam evaporation in vacuum.

2.2. Functionalization of SPR chips with alkanethiols

SPR chips were immersed in a 200 μM ethanoic solution (ethanol for spectroscopy, Merck, Czech Republic) of alkanethiols HS$(CH_2)_{11}(EG)_6OCH_2$-COOH (AT-EG_6-COOH), HS$(CH_2)_{11}(EG)_4$OH (AT-EG_4-OH) (Prochimia, Poland), or 16-mercaptodecanoic acid (16-MHDA) (Sigma Aldrich, USA). The chips were stored overnight in dark conditions at room temperature. Prior to each measurement the chips were washed with ethanol and immersed in absolute ethanol for 30 min. The chip was then subsequently washed with absolute ethanol and deionized water and dried with nitrogen.

2.3. Determination of surface concentration of thiols with SPR

SPR chips were cleaned with a UV-ozone cleaner for 5 min, washed with ethanol and water, dried with nitrogen, and mounted on the SPR sensor. The fluidic chambers were flooded with 10 mM Tris buffer (pH 7.4) and reflectance spectra were recorded (Fig. S1). The chips were then removed from the SPR sensor instrument and functionalized with AT-EG_4-OH following the procedure described above. Subsequently, the chips were mounted on the SPR sensor and the SPR wavelength in Tris was recorded. The difference between the SPR wavelength before and after the adsorption of AT-EG_4-OH was determined to be 13.2 ± 0.6 nm (measured on 3 SPR chips and 4 different positions). For this SPR setup a 1 nm SPR wavelength shift corresponds a change in biomolecular surface coverage of 17 ng cm^{-2} (Homola, 2006).

2.4. pKa measurements and calculation of ΔSPR^C

The 10 mM buffer solutions were prepared using Millipore Q water (18.0 MΩ cm, Milli-Q), and all reagents were purchased from Sigma Aldrich in molecular biology grade or higher. The pH of the buffers was adjusted at 25 °C by adding small amounts of 1 M HCl or 100 mM NaOH. The pH of the buffers used for determination of pKa were as follows: Glycine pH 2.2 and 3; Sodium acetate pH 4, 4.5, 5, and 5.5; MES pH 5.5, 6.5 and 6; HEPES pH 7, 7.4 and 8; Tris pH 7.4, 8.2 and 9; Bicine pH 9 and 10. The measurements were performed with a SPR chip functionalized with AT-EG_6-COOH, AT-EG_4-OH, or 16-MHDA. The SPR wavelength was tracked while various buffers were injected into the flow-cell. Starting with Glycine (pH 2.2, 0.2 mM), we injected different 0.2 mM buffers of various pH for 10 or more minutes until a stable SPR sensor response was obtained, followed by a 5-min injection of Glycine. The measurements were performed on at least 3 SPR chips, each providing 2 measurement channels.

Net SPR wavelength shift due to SPR surface charging (ΔSPR^C) was calculated as $\Delta SPR^C = \Delta SPR_X - \Delta SPR_{OH}$, where ΔSPR_X is the SPR shift between two solutions measured on a carboxyl-terminated SAM (AT-EG_6-COOH or 16-MHDA); ΔSPR_{OH} is the SPR shift between respective

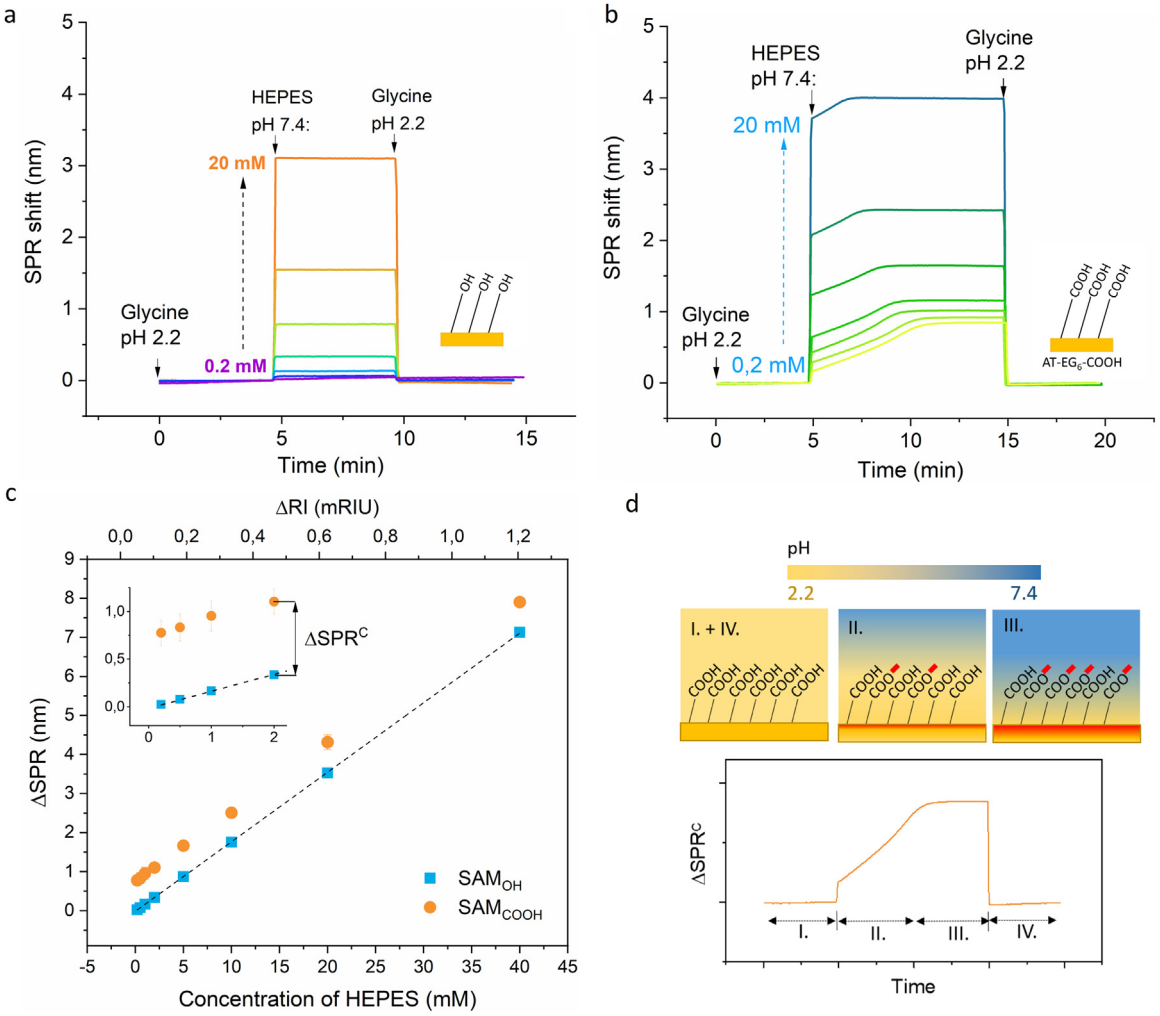

Fig. 1. SPR wavelength shift caused by deprotonation of carboxylic moieties on SAMs. a, b) Temporal SPR sensor response to subsequent injections of 0.2 mM Glycine (pH 2.2) and HEPES buffers (pH 7.4) of various concentrations (0.2, 0.5, 1, 2, 5, 10 and 20 mM). Arrows indicate the injection of respective buffers. The SPR chip was functionalized with (a) SAM_{OH} or (b) SAM_{COOH}. c) The relative SPR shifts between the 0.2 mM Glycine and HEPES (pH 7.4) of various concentrations measured on SPR chips with SAM_{COOH} (circles) or SAM_{OH} (squares). The SPR shift was measured after stabilization of the temporal SPR response in HEPES. Refractive indices of the solutions at 750 nm were measured with a refractometer. d) Schematic diagram of the temporal SPR sensor response shown in (b) with hypothesized processes: I. At pH 2.2, the carboxylic groups are fully protonated; II. After switching to pH 7.4, pH in the proximity of the SAM_{COOH} gradually increases, inducing the ionization of carboxylic groups and a shift in SPR wavelength; III. pH close to the SPR surface reaches a constant value; IV. The carboxylic groups quickly become protonated after change of the medium back to buffer with pH 2.2.

solutions measured on chips having neutral SAM_{OH} (AT-EG_4-OH). ΔSPR_{OH} reflects the SPR wavelength shift due to a difference in RI of the solutions.

2.5. Multilayer model of SPR sensor

We used the Transfer Matrix Method (Born et al., 1999) to estimate the reflection of p-polarized light and predict the shift of SPR wavelength caused by the deprotonation of a carboxyl-terminated SAM. In the case of a neutral biomolecular layer (COOH terminated) we considered a multilayer system consisting of: 1) a semi-infinite prism (BK7 glass, RI = 1.51), 2) a 50 nm-thick gold or silver film (RI of gold and silver taken from (Johnson and Christy, 1972)), 3) a 3.5 nm-thick (Šípová et al., 2018) SAM layer (RI = 1.46, the RI was set so the calculated SPR shift due to adsorption of SAM agrees with experimental data), and 4) a semi-infinite layer of water (RI = 1.33). The 1.5 nm titanium layer was neglected in the calculations due to a large uncertainty in the optical parameters of the layer and moreover, a small anticipated influence on the outcome of the simulations. In the case of a negatively charged biomolecular layer (COO^- terminated), we further divided the metal layer into 3 regions: 3a) a bottom layer with charge $\rho = \sigma/2$ and 0.1 nm thickness, 3b) a 49.8 nm thick gold layer, and 3c) a top layer with charge $\rho = -\sigma/2$ and 0.1 nm thickness, where σ is the surface charge of a fully protonated layer of carboxylic groups. To mimic the experimental configuration, we chose the angle of incidence of light so that the SPR dip in the spectrum of p-polarized light of neutral surfaces was positioned at 750 nm (i.e., 67.505° for gold and 65.83° for silver).

2.6. PM-IRRAS

PM-IRRAS spectra of alkanethiol SAMs on gold surfaces were recorded using a NICOLET 6700 FT-IR spectrometer with a photoelastic modulation (PEM) module. The sample was illuminated by a beam of light incident on the surface at an angle of 82°. A ZnSe grid polarizer and a ZnSe photoelastic modulator, modulating the incident beam between p- and s-polarizations (HINDS Instruments, PEM 90, modulation frequency = 37 kHz), were placed in front of the sample. The light reflected from the sample was focused on a nitrogen-cooled MCT (Mercury–Cadmium–Telluride) detector. The PM-IRRAS signal was

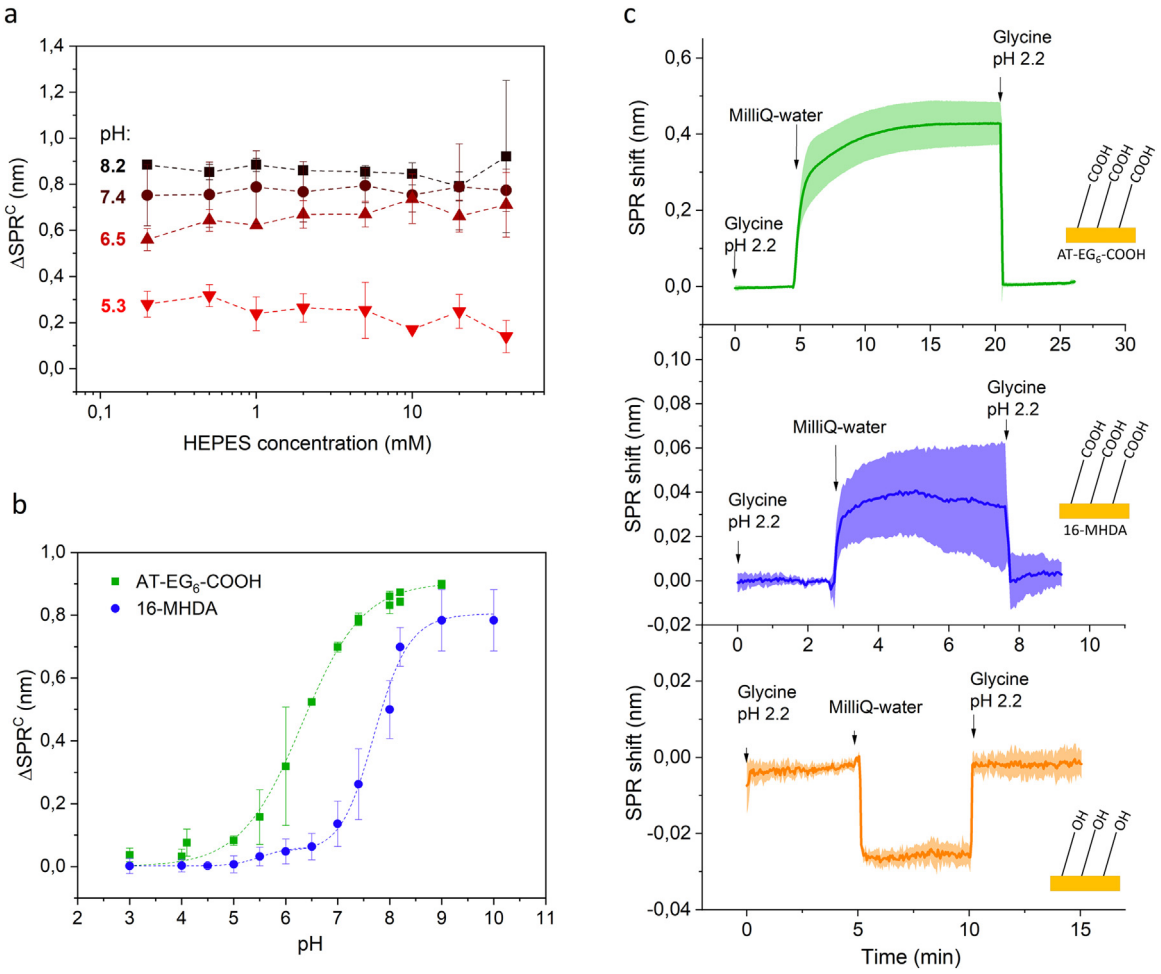

Fig. 2. Charge-induced SPR wavelength shift (ΔSPR^C) in water and buffers of various pH is proportional to the degree of ionization of carboxyl moieties on SAM_{COOH} a) SPR wavelength shift between 0.2 mM Glycine (pH 2.2) and HEPES of various pH and concentrations caused by ionization of carboxylic end-groups on SAM_{COOH}. b) ΔSPR^C in 0.2 mM buffers of various pH. The SPR chip surface was functionalized with either SAM_{COOH} (squares) or SAM_{MHDA} (circles). ΔSPR^C was measured relative to 0.2 mM Glycine (pH 2.2). The pKa of the carboxyl groups was determined from fits to a logistic function (dashed lines): 6.31 and 7.71 for SAM_{COOH} and SAM_{MHDA}, respectively. Error bars represent standard deviation of at least 6 measurements on 3 different SPR chips. c) Temporal SPR sensor response to sequential injections of 0.2 mM Glycine (pH 2.2), ultra-pure water, and Glycine. Arrows indicate injection. The SPR chips were functionalized with SAM_{COOH} (top), SAM_{MHDA} (middle), and SAM_{OH} (bottom). Data were collected in 6 different measurements and the shaded areas represent the standard deviation of measurement.

obtained as follows: $\Delta R/R = (Rp - Rs)/(Rp + Rs)$, where Rp and Rs corresponded to the reflectivity of p- and s-polarized light. The spectra were obtained as the average value of 100 scans recorded with 4 cm^{-1} resolution.

The SPR chips were immersed in 200 μM solution of a mixed alkanethiols in ethanol ($AT\text{-}EG_6\text{-}COOH$ and $AT\text{-}EG_4\text{-}OH$) at molar ratios of 0:1, 1:999, 1:199, 1:99, 1:19, 3:7, and 1:0, respectively. After removing each chip from ethanolic solution, the surface was rinsed with ethanol (96%), water, and dried with a stream of nitrogen. During each experiment the PEM chamber was supplied with dry air to minimize the effect of moisture. The relative concentration of $AT\text{-}EG_6\text{-}COOH$ in each SAM was determined from the area of the absorption peak at 1110–1146 cm^{-1}, corresponding to the asymmetric C-O-C stretching mode within ethylene-glycol groups.

3. Results

3.1. Negative charges on SAM carboxylic groups cause a SPR shift

To determine whether the spectral position of SPR is influenced by the electrostatic charge of immobilized molecules, we measured the SPR sensor response while varying the conditions of the medium (pH, ionic strength) in contact with SPR chips functionalized with SAMs of carboxyl- ($AT\text{-}EG_6\text{-}COOH$) or hydroxyl- ($AT\text{-}EG_4\text{-}OH$) terminated alkanethiols (SAM_{COOH} or SAM_{OH}, respectively). Initial injections of pH 2.2 glycine (ensuring that the SAM_{COOH} layer was fully protonated) were followed by injections of a buffer having physiological pH (HEPES, pH 7.4, various concentrations). We observed a qualitative difference in the temporal responses between surfaces coated with SAM_{OH} (Fig. 1a) and those coated with SAM_{COOH} (Fig. 1b). The temporal SPR sensor response of the SAM_{OH} chip (Fig. 1a) exhibits standard behavior, where an abrupt SPR shift occurs after the injection of HEPES buffer (due to the RI difference between the two solutions) and quickly reaches a steady-state as soon as the buffers are fully exchanged in the flow-cell chamber (within few seconds). We observed that changes in the SPR signal (ΔSPR) scaled linearly with changes in refractive index (ΔRI) between the glycine and the various HEPES buffers (Fig. 1c). For the SAM_{OH} chip we calculated a bulk refractive index sensitivity (defined as $d\lambda/dn$) to be: 5774 ± 11 nm/RIU; ΔSPR for 0 mM concentration of HEPES (pure water) was determined to be −0.015 ± 0.003 nm.

The temporal SPR sensor response of the SAM_{COOH} chip (Fig. 1b) exhibited more complex behavior with respect to the SAM_{OH} chip. After an initial abrupt change due to the HEPES injection, the SPR wavelength exhibited a further gradual increase, finally reaching a steady-state after several minutes (we discuss this effect further in the text). Moreover, we observed increased SPR shifts for the SAM_{COOH} chip with

respect to the SAM_{OH} chip. The major difference between the measurements shown in Fig. 1a and b are the moieties on the SAMs, therefore the increased SPR wavelength shift recorded on the surface coated with SAM_{COOH} is most likely caused by the deprotonation of carboxyl moieties at pH 7.4. Other differences, such as the different number of ethylene-glycol groups in each alkanethiol chain (6 in AT-EG_6-COOH vs. 4 in AT-EG_4-OH), or potential differences in the SAM packing density, are believed to have only minor effect.

We fit the (steady) SPR shifts for the SAM_{COOH} with linear regression (Fig. 1c). Calculated bulk refractive index sensitivity is $d\lambda/dn$ = 5759 ± 19 nm/RIU, which is very similar to that taken measurements on neutral SAM_{OH} (Fig. 1c). However, the intercept of this data (corresponding to 0 mM of HEPES) is considerably higher, calculated as 0.75 ± 0.01 nm. When we subtract the SPR wavelength shift due to difference in the refractive index of water and 0.2 mM Glycine (−0.015 nm), we obtain the total SPR shift caused by the charging of the carboxylic groups in pH 7.4: SPR^C = 0.765 ± 0.013 nm.

To confirm the hypothesis that the deprotonation of carboxylic groups on SAM_{COOH} causes a shift of the SPR wavelength, we measured the SPR sensor response to HEPES buffer over a pH range of 5.3–8.2, which is expected to yield a variable degree of ionization of carboxyl groups. We observed that ΔSPR^C increases with increasing pH, but depends only weakly on the buffer concentration (Fig. 2a). To extend the range of available pH values, we further employed other 0.2 mM buffers that allowed us to determine ΔSPR^C over a pH range of 3–9. We observed that ΔSPR^C is close to zero for buffers of pH 4 and lower, and increases with increasing pH due to the gradual deprotonation of carboxylic groups (Fig. 2b). A plateau (at a value of 0.9 nm) was reached for buffers of pH 8 and higher. These data were fit to a logistic function, yielding a pKa value for the carboxylic groups on SAM_{COOH} of 6.31 ± 0.02.

We performed similar measurements on SPR chips functionalized with 16-MHDA (SAM_{MHDA}, Fig. 2b, circles). We observed that ΔSPR^C is equal to zero for buffers with pH values up to 4.5, where further increases in pH lead to two "shoulders," the first in the range of pH 6, and the second in the range of pH ≥ 9. We fit these data with two logistic functions: one in the pH range 3–6.5 and another in the pH range 6–10, which yielded two pKa values of 5.54 ± 0.08 and 7.71 ± 0.09. These results agree well with previous work, where the surface pKa of carboxylic groups on carboxyl-terminated SAMs has been found to be in the range of 5–9 (Fears et al., 2008; Marmisolle et al., 2013; Sanders et al., 2008), depending on the length of alkyl chain and experimental method used for its determination.

The difference between the two data sets in Fig. 2b can be attributed to the nature of each coating: the carboxyl groups on SAM_{COOH} are significantly more acidic than the carboxyls on SAM_{MHDA}, which is a result of the higher electronegativity of ethylene-glycol on AT-EG_6-COOH compared to the aliphatic carbohydrate chain of 16-MHDA. The presence of two acid-base equilibria of a carboxylic acid-functionalized surface has been previously reported (Gershevitz and Sukenik, 2004; Konek et al., 2004); the higher pKa value is typically linked to the deprotonation of laterally hydrogen-bonded COOH groups, and the lower one to the deprotonation of COOH groups that are not hydrogen-bonded to one another (Konek et al., 2004).

To exclude the ionic mechanism as a cause of the SPR shift, we performed similar experiments as shown on Fig. 1a and b, but used ultrapure water instead of HEPES buffer. Fig. 2c shows the temporal SPR response to the injection of Glycine, ultrapure water, and Glycine. There is a pronounced difference in SPR response measured on SPR chips coated with SAM_{COOH} (top), SAM_{MHDA} (middle), and SAM_{OH} (bottom). Despite the lower refractive index of water compared to the refractive index of 0.2 mM Glycine, the SPR responses measured on both chips with carboxyl-terminated SAMs show positive SPR shifts when the solution is changed from Glycine to water. Similar to previous experiments (Fig. 1a), the SPR sensor response for chips coated with SAM_{OH} showed anticipated trends regarding the exchange of solutions with respective refractive indexes. Even though the negatively charged carboxyl groups attract H+ and repel OH- and result in a local imbalance of H^+ ions close to the surface (Brüesch and Christen, 2004), this imbalance is likely to have only a minor effect on the local RI due to small size of the H^+ ions. Moreover, as ultrapure water contains very little ions, we can exclude the ionic mechanism as a cause of the observed SPR wavelength shifts measured on SPR chips coated with carboxyl-terminated SAMs.

Using measurements of ΔSPR between the glycine and water (ΔSPR_{COOH} = 0.43 ± 0.06 nm, ΔSPR_{MHDA} = 0.04 ± 002 nm, and ΔSPR_{OH} = −0.031 ± 0.008), we calculated the respective SPR shift due to surface charging ($\Delta SPR_X{}^C = \Delta SPR_X - \Delta SPR_{OH}$) as ΔSPR^C_{COOH} = 0.46 ± 0.06 nm and ΔSPR^C_{MHDA} = 0.07 ± 0.02 nm. These data were used with the fitted curves in Fig. 2b to calculate the pH of pure water: from ΔSPR^C_{COOH} we obtain pH_{water} = 6.3 (higher and lower boundaries are 6.5 and 6.3, respectively) and from ΔSPR^C_{MHDA} we obtain pH_{water} = 6.7 (higher and lower boundaries are 6.9 and 5.8, respectively). The calculated pH is lower that the theoretical value of 7 of ideally pure water. We believe that this difference can be partially attributed to both the air dissolved in the water as well as to the carboxyl moieties on the surface, which decrease the local pH in their proximity (Fears et al., 2008).

We note here that the charging of SPR surfaces coated with SAM_{COOH} and SAM_{MHDA} is a gradual process, especially in ultrapure water, where the former surface takes more than 10 min for the SPR sensor response to reach a steady value. We hypothesize that this delay reflects the evolution of pH in the proximity of the surface because of the high surface concentration of carboxylic groups. It is in part due to mass transport of OH- and H+ ions from the bulk solution towards the surface of the SPR sensor that is carried out by convection and diffusion (Squires et al., 2008). The pH equilibration is further slowed down by dissociation of protons from carboxyl moieties on the surface. A similar gradual deprotonation was observed in pH 7.4 HEPES buffers (Fig. 1b, d); however, in that case, the time necessary for reaching equilibration was shorter: approximately 5 min for 0.2 mM HEPES and only 2 min for 20 mM HEPES. We can conclude that the presence of buffer molecules accelerates the pH equilibration close to the immobilized molecules, and that equilibration time decreases with increasing buffer concentration. These results illustrate the ability of SPR sensor method to measure ionization processes in real time.

3.2. The electronic mechanism

To explore the hypothesis that the observed SPR wavelength shifts resulting from biomolecular charging were caused by an electromagnetic mechanism, we compared experimental results to those from a theoretical model that considers changes in the density of conductive electrons in the metal layer. In this model, the deprotonated carboxylic groups on the SAM are treated as a charge plane parallel to the SPR chip surface. As follows from Gauss' law of electrostatics, a plane of surface charge σ induces a charge $-\sigma/2$ in the neighboring surface and $\sigma/2$ at the distant surface of the metal layer, respectively. In this approach we neglect the screening by counterions in solution, and therefore σ is determined by the concentration of deprotonated carboxyl-terminated alkanethiols in the SAM. We experimentally determined the concentration of alkanethiols in SAM_{OH} coatings to be $(3.8 \pm 0.2)\cdot 10^{14}$ molecules cm^{-2}, which corresponds well with the values reported in literature for alkanethiol SAMs (Love et al., 2005). Assuming that the surface concentrations of molecules in SAM_{COOH} are similar, the surface charge of a fully deprotonated SAM_{COOH} is $\sigma = -60 \pm 3.6\ \mu C\ cm^{-2}$. The induced charge on the metal boundary is realized by change in the electron density on the surface of the metal. The thickness of the layer within which the change occurs is equal to the penetration depth d of the quasi-static electromagnetic field into the metal (in case of gold and silver $d \leq 0.1$ nm). We assume that the dielectric constant of gold at optical frequencies is determined mainly by the contribution of free

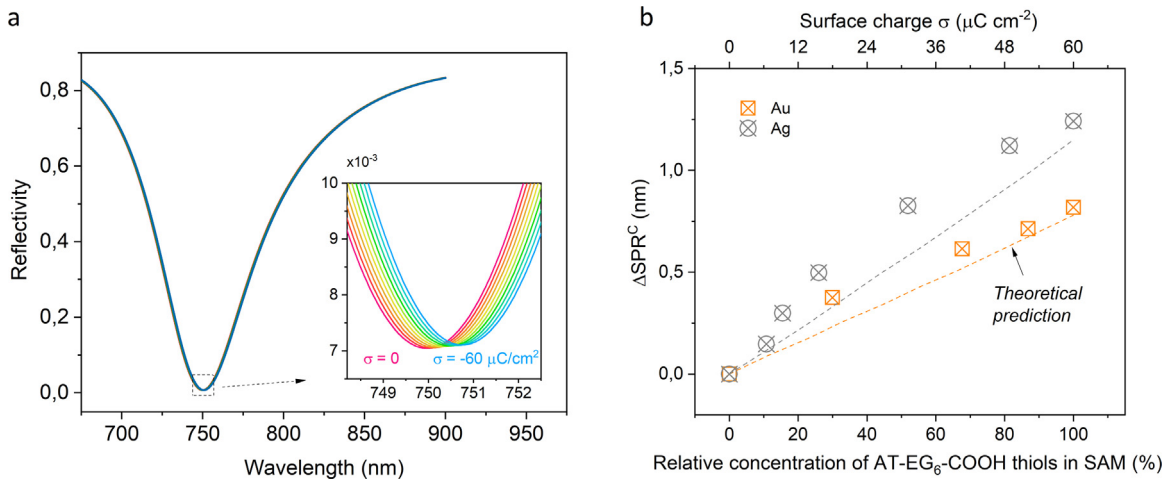

Fig. 3. SPR shift caused by an electronic mechanism. a) Theoretical reflectivity of p-polarized light on a multilayer SPR structure containing a neutral biomolecular layer ($\sigma = 0$) and biomolecular layers with negative surface charge densities from $\sigma = -60\,\mu C\,cm^{-2}$ to $\sigma = -6\,\mu C\,cm^{-2}$ (in increments of $6\,\mu C\,cm^{-2}$). $\sigma = -60\,\mu C\,cm^{-2}$ corresponds to a surface charge of fully deprotonated SAM_{COOH}. Inset shows detail of the SPR dip in reflectivity. b) Theoretical prediction of charge-induced SPR shift (ΔSPR^C) calculated on silver and gold films. The points represent experimental data obtained using SPR chips functionalized with binary mixtures of AT-EG_6-COOH and AT-EG_4-OH. The ΔSPR^C was measured between 0.2 mM Glycine (pH 2.2) and 0.2 mM Tris (pH 7.4).

electrons in the metal. Consequently, the dielectric constant of the metal in the thin surface layer can be expressed as $\varepsilon_m = \varepsilon_{m0} + \Delta\varepsilon_m$ (Lioubimov et al., 2004), where ε_{m0} is the unperturbed dielectric constant and $\Delta\varepsilon_m$ is the change caused by the external charge-induced variation in electron density in the metal. $\Delta\varepsilon_m$ can then be expressed as (Mcintyre, 1973):

$$\Delta\varepsilon_m = \frac{\rho}{edn}(\varepsilon_{m0} - 1), \quad (1)$$

where n is the density of free electrons in the metal ($n = 5.9 \cdot 10^{22}\ cm^{-3}$ in gold, $5.86 \cdot 10^{22}\ cm^{-3}$ in silver (Kittel, 2005)), e is the elementary charge, and ρ is the surface charge of the layer ($\rho = \pm\ \sigma/2$).

The calculated reflectivity of p-polarized light for SPR chips containing a neutral ($\sigma = 0$) and fully deprotonated SAMs of carboxyl-terminated alkanethiols ($\sigma = -60\,\mu C\,cm^{-2}$) show SPR dips that are shifted by 0.78 nm from each other (Fig. 3), showing very good agreement with experimental data ($\Delta SPR^C = 0.765$ in pH 7.4). We also calculated ΔSPR^C for lower surface charge densities; the results suggest that ΔSPR^C displays direct proportionality to σ within the range of experimental conditions (Fig. 3b). Similar calculations were performed for silver SPR chips, where we found that the sensitivity of the SPR to changes in surface charge is approximately 1.5 times higher than that for gold SPR chips. If we consider the lowest detectable SPR shift as 3 times the standard deviation of the baseline noise (0.01 nm for the SPR sensor used in this study), the theoretical limit of detection for the surface charge is $775\,nC\,cm^{-2}$ for gold and $529\,nC\,cm^{-2}$ for silver SPR films.

To confirm these results experimentally, we functionalized gold and silver SPR surfaces with SAMs of various molar ratios of AT-EG_6-COOH and AT-EG_4-OH to obtain SAMs with different concentrations of carboxylic groups. The relative concentration of the AT-EG_6-COOH thiols in each SAM was determined by PM-IRRAS. From the data shown in Fig. 3b, it can be seen that the measured ΔSPR^C between the pH 2.2 and 7.4 agrees very well with the theoretical model for high molar ratios of AT-EG_6-COOH, and slightly deviates from a linear trend predicted by the theory for lower molar ratios of carboxylic group. The deviation from linear trend can be explained by incomplete deprotonation of carboxylic groups in SAMs with a high content of carboxyl-terminated alkanethiols which is caused by steric hindrance (Aureau et al., 2008).

3.3. Ionic mechanism

To investigate the potential role of an ionic mechanism, we studied the interaction between small ions with a negatively charged SPR sensor surface and examined the extent to which it affects the SPR spectral position. We first utilized SPR chips coated with SAM_{MHDA} that exhibit a relatively small negative surface charge in ultrapure water (as showed earlier ΔSPR^C ~0.07 nm in water). Initial injections of pH 2.2 glycine were followed by injections of either aqueous NaCl or $MgCl_2$ solutions for 5 min, followed by a second injection of glycine. We observed that even micromolar concentrations of $MgCl_2$ caused measurable ΔSPR^C (Fig. 4a); we believe that this can be attributed to ion accumulation in the proximity of the carboxyl-terminated SAM. We note that the SPR spectral position immediately returns to its initial level at the second injection of glycine, suggesting a fast dissociation of the ionic layer. Fig. 4b summarizes ΔSPR^C measured from 5 min-injections of both NaCl and $MgCl_2$ solutions over the SAM_{MHDA}. It can be seen that both NaCl and $MgCl_2$ cause SPR wavelength shifts that increase with the salt concentration, reaching up to 2.5 nm (in the case of 100 mM $MgCl_2$). The NaCl solutions cause much lower SPR shifts than $MgCl_2$ of the same concentrations, and measurable ΔSPR^C can be seen only for NaCl concentrations higher than 10 mM. We observed similar behavior in theoretical calculations for double layers formed above a charged surface. For this we calculated SPR shifts using the Gouy–Chapman theory for surface potentials of $\phi = 40$ and 100 mV, corresponding to a double-layer of monovalent and divalent ions, respectively (for details, see Supplementary materials). The calculated ΔSPR^C for surface potential $\phi = 100$ mV shown in Fig. 4c are qualitatively similar to those in Fig. 4b; thus, the formation of a double-layer can therefore be a plausible explanation for the observed ΔSPR^C in $MgCl_2$ and NaCl solutions for SAM_{MHDA} surfaces.

To study a system where both ionic and electronic mechanisms are present, we measured the ΔSPR_C in NaCl and $MgCl_2$ solutions on SPR surface coated with SAM_{COOH} (Fig. 4d). As shown earlier for these surfaces, the value of ΔSPR^C in ultrapure water is about 0.47 nm, indicating that approximately half of the carboxylic groups are deprotonated. We observed that ΔSPR^C increased with increasing $MgCl_2$ concentration, reaching a plateau at the concentration of $MgCl_2$ of about 5 mM. In contrast to $MgCl_2$, ΔSPR^C is weakly dependent on the NaCl concentration below 10 mM and increases at higher concentrations. This data suggests that ΔSPR^C is composed of both electronic and ionic contributions. Both these processes are in dynamic equilibrium and it is

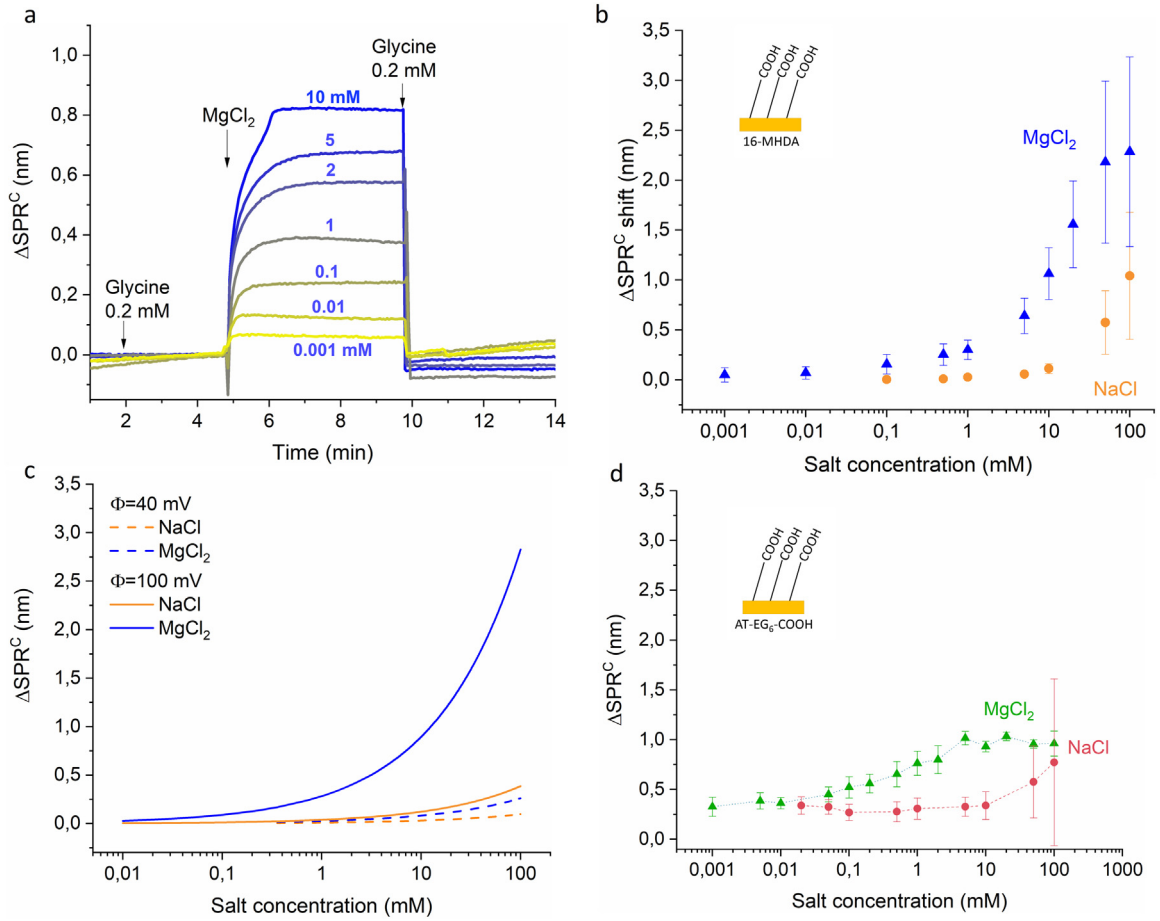

Fig. 4. Formation of an ionic double-layer causes a SPR shift. a) Temporal SPR sensor response corresponding to the formation of a double-layer formation in $MgCl_2$ solutions over a SPR surface functionalized with SAM_{MHDA}. Arrows indicate injection of respective solutions. Data were corrected for refractive index differences. b) and d) Charge-induced SPR wavelength shift (ΔSPR^C) caused by the formation of double layers of NaCl and $MgCl_2$ formed over (b) SAM_{MHDA} and (d) SAM_{COOH}. The data were obtained from measurements on 3 chips. c) SPR wavelength shift calculated using the Gouy-Chapman model for various surface potentials.

possible that the induced charge on gold can screen the long-range interaction of ions with the surface, thus hampering the accumulation of ions at higher concentrations.

4. Conclusions

In this work we show that presence of negative static charges on (or near) the surface of an SPR chip can potentially result in significant shifts in the SPR wavelength. Furthermore, we identify two major mechanisms responsible for this effect: 1) an ionic mechanism, resulting from the accumulation of ions with opposite charge in the proximity of a charged biomolecular layer, and 2) an electronic mechanism, resulting from changes in electron density at the surface of metal. Our results suggest that the electronic mechanism is dominant in solutions of low ionic strength, while at high ionic strengths both mechanisms contribute to the SPR change. Although the effect of surface charge on response of SPR biosensors has been overlooked so far, it is clear from our study that it may have impact on the results of many SPR experiments. Therefore, charge-induced SPR changes should be considered in biomolecular SPR sensing, determination of surface concentration of bound ligands, and interaction stoichiometry. Alternatively, the effect of surface charges can be reduced by optimizing the experimental conditions (e.g. choosing low-ionic strength buffers at lower pH) in which the molecules/functional coating possess a net neutral charge. On the other hand, it should be noted that sensitivity of SPR to charges at the metal surface provides a potentially interesting avenue to new applications of SPR biosensors, such as quantification of biomolecular charges as well as the study of acid-base equilibria for functional groups in biomolecular films. These phenomena are difficult to access with other methods yet are of great importance in numerous areas of material science and surface chemistry.

Acknowledgements

This work was supported by the Czech Science Foundation, Czech Republic, under contract #P205/12/G118.

Appendix A. Supplementary material

Supplementary data associated with this article can be found in the online version at doi:10.1016/j.bios.2018.11.002.

References

Abb, M., Wang, Y.D., Papasimakis, N., de Groot, C.H., Muskens, O.L., 2014. Surface-enhanced infrared spectroscopy using metal oxide plasmonic antenna arrays. Nano Lett. 14 (1), 346–352.

Aureau, D., Ozanam, F., Allongue, P., Chazalviel, J.N., 2008. The titration of carboxyl-terminated monolayers revisited: in situ calibrated Fourier transform infrared study of well-defined monolayers on silicon. Langmuir 24 (17), 9440–9448.

Barnes, W.L., Dereux, A., Ebbesen, T.W., 2003. Surface plasmon subwavelength optics. Nature 424 (6950), 824–830.

Berini, P., De Leon, I., 2012. Surface plasmon-polariton amplifiers and lasers. Nat. Photonics 6 (1), 16–24.

Born, M., Wolf, E., Bhatia, A.B., 1999. Principles of Optics: Electromagnetic Theory of Propagation, Interference and Diffraction of Light. Cambridge University Press, Cambridge.

Brüesch, P., Christen, T., 2004. The electric double layer at a metal electrode in pure water. J. Appl. Phys. 2846–2856.
Dahlin, A.B., Zahn, R., Voros, J., 2012. Nanoplasmonic sensing of metal-halide complex formation and the electric double layer capacitor. Nanoscale 4 (7), 2339–2351.
de Feijter, J.A., Benjamins, J., Veer, F.A., 1978. Ellipsometry as a tool to study the adsorption of synthetic and biopolymers at the air-water interface. Biopolymers 17, 1759–1772.
Fang, Y., Sun, M., 2015. Nanoplasmonic waveguides: towards applications in integrated nanophotonic circuits. Light: Sci. Appl. 4 (6), e294.
Fears, K.P., Creager, S.E., Latour, R.A., 2008. Determination of the surface pK of carboxylic- and amine-terminated alkanethiols using surface plasmon resonance spectroscopy. Langmuir 24 (3), 837–843.
Fischer, M.J.E., 2010. Amine coupling through EDC/NHS: a practical approach. In: Mol, N.J., Fischer, M.J.E. (Eds.), Surface Plasmon Resonance: Methods and Protocols. Humana Press, Totowa, NJ, pp. 55–73.
Foley, K.J., Shan, X., Tao, N.J., 2008. Surface impedance imaging technique. Anal. Chem. 80 (13), 5146–5151.
Gershevitz, O., Sukenik, C.N., 2004. In situ FTIR-ATR analysis and titration of carboxylic acid-terminated SAMs. J. Am. Chem. Soc. 126 (2), 482–483.
Homola, J., 2006. Surface Plasmon Resonance Based Sensors. Springer-Verlag, Germany, Berlin.
Johnson, P.B., Christy, R.W., 1972. Optical-constants of noble-metals. Phys. Rev. B 6 (12), 4370–4379.
Karlsson, R., 2004. SPR for molecular interaction analysis: a review of emerging application areas. J. Mol. Recognit. 17 (3), 151–161.
Kawata, S., Inouye, Y., Verma, P., 2009. Plasmonics for near-field nano-imaging and superlensing. Nat. Photonics 3 (7), 388–394.
Kittel, C., 2005. Introduction to Solid State Physics, 8th ed. Wiley, New York.
Konek, C.T., Musorrafiti, M.J., Al-Abadleh, H.A., Bertin, P.A., Nguyen, S.T., Geiger, F.M., 2004. Interfacial acidities, charge densities, potentials, and energies of carboxylic acid-functionalized silica/water interfaces determined by second harmonic generation. J. Am. Chem. Soc. 126 (38), 11754–11755.
Lioubimov, V., Kolomenskii, A., Mershin, A., Nanopoulos, D.V., Schuessler, H.A., 2004. Effect of varying electric potential on surface-plasmon resonance sensing. Appl. Opt. 43 (17), 3426–3432.
Love, J.C., Estroff, L.A., Kriebel, J.K., Nuzzo, R.G., Whitesides, G.M., 2005. Self-assembled monolayers of thiolates on metals as a form of nanotechnology. Chem. Rev. 105 (4), 1103–1169.
Mariani, S., Minunni, M., 2014. Surface plasmon resonance applications in clinical analysis. Anal. Bioanal. Chem. 406 (9–10), 2303–2323.
Marmisolle, W.A., Capdevila, D.A., de la Llave, E., Williams, F.J., Murgida, D.H., 2013. Self-assembled monolayers of NH2-terminated thiolates: order, pK(a), and specific adsorption. Langmuir 29 (17), 5351–5359.
Mcintyre, J.D., 1973. Electrochemical modulation spectroscopy. Surf. Sci. 37 (1), 658–682.
Novo, C., Funston, A.M., Gooding, A.K., Mulvaney, P., 2009. Electrochemical charging of single gold nanorods. J. Am. Chem. Soc. 131 (41), 14664.
Nylander, C., Liedberg, B., Lind, T., 1982. Gas-detection by means of surface-plasmon resonance. Sens. Actuators 3 (1), 79–88.
Puiu, M., Bala, C., 2016. SPR and SPR imaging: recent trends in developing nanodevices for detection and real-time monitoring of biomolecular events. Sensors 16 (6), 870.
Sanders, W., Vargas, R., Anderson, M.R., 2008. Characterization of carboxylic acid-terminated self-assembled monolayers by electrochemical impedance spectroscopy and scanning electrochemical microscopy. Langmuir 24 (12), 6133–6139.
Šípová, H., Ševců, V., Kuchař, M., Ahmad, J.N., Mikulecký, P., Osička, R., Malý, P., Homola, J., 2012. Surface plasmon resonance biosensor based on engineered proteins for direct detection of interferon-gamma in diluted blood plasma. Sens. Actuators B-Chem. 174, 306–311.
Šípová, H., Shao, L., Odebo Länk, N., Andrén, D., Käll, M., 2018. Photothermal DNA release from laser-tweezed individual gold nanomotors driven by photon angular momentum. ACS Photonics.
Špringer, T., Piliarik, M., Homola, J., 2010. Real-time monitoring of biomolecular interactions in blood plasma using a surface plasmon resonance biosensor. Anal. Bioanal. Chem. 398 (5), 1955–1961.
Squires, T.M., Messinger, R.J., Manalis, S.R., 2008. Making it stick: convection, reaction and diffusion in surface-based biosensors. Nat. Biotechnol. 26 (4), 417.
Su, X.D., Wu, Y.J., Robelek, R., Knoll, W., 2005. Surface plasmon resonance spectroscopy and quartz crystal microbalance study of streptavidin film structure effects on biotinylated DNA assembly and target DNA hybridization. Langmuir 21 (1), 348–353.
Wang, S.P., Huang, X.P., Shan, X.N., Foley, K.J., Tao, N.J., 2010. Electrochemical surface plasmon resonance: basic formalism and experimental validation. Anal. Chem. 82 (3), 935–941.
Wijaya, E., Lenaerts, C., Maricot, S., Hastanin, J., Habraken, S., Vilcot, J.-P., Boukherroub, R., Szunerits, S., 2011. Surface plasmon resonance-based biosensors: from the development of different SPR structures to novel surface functionalization strategies. Curr. Opin. Solid State Mater. Sci. 15 (5), 208–224.